HHS Public Access

Author manuscript

Biochemistry. Author manuscript; available in PMC 2018 November 03.

Published in final edited form as:

Biochemistry. 2018 February 20; 57(7): 1212–1218. doi:10.1021/acs.biochem.7b01272.

Molecular Interactions between a Fluoride Ion Channel and Synthetic Protein Blockers

Daniel L. Turman, **Abraham Z. Cheloff**, **Alexis D. Corrado**, **Jacob T. Nathanson**, and **Christopher Miller***

Department of Biochemistry, Howard Hughes Medical Institute, Brandeis University, 415 South Street, Waltham, Massachusetts 02453, United States

Abstract

Fluoride ion channels of the Fluc family selectively export F^- ions to rescue unicellular organisms from acute F^- toxicity. Crystal structures of bacterial Fluc channels in complex with synthetic monobodies, fibronectin-derived soluble β-sandwich fold proteins, show 2-fold symmetric homodimers with an antiparallel transmembrane topology. Monobodies also block Fluc F^- current via a pore blocking mechanism. However, little is known about the energetic contributions of individual monobody residues to the affinity of the monobody—channel complex or whether the structural paratope corresponds to functional reality. This study seeks to structurally identify and compare residues interacting with Fluc between two highly similar monobodies and subjects them to mutagenesis and functional measurements of equilibrium affinities via a fluorescence anisotropy binding assay to determine their energetic contributions. The results indicate that the functional and structural paratopes strongly agree and that many Tyr residues at the interface, while playing a key role in affinity, can be substituted with Phe and Trp without large disruptions.

Graphical Abstract

*Corresponding Author: cmiller@brandeis.edu.

Supporting Information

The Supporting Information is available free of charge on the ACS Publications website at DOI: 10.1021/acs.biochem.7b01272.

FA equilibrium binding isotherms for S9 and S12 mutants with solid curve fits to eq 1, where points and error bars represent the mean ± SEM from three experiments (PDF)

The authors declare no competing financial interest.

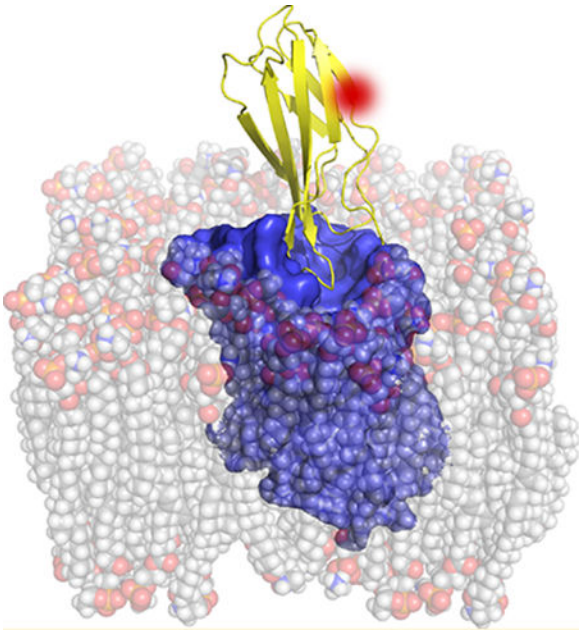

The F^- ion pervades the aqueous environment at concentrations of 10–100 μM, and within weakly acidic niches, accumulation of F^- in microorganisms threatens to inhibit enzymes central to DNA synthesis and glycolytic energy metabolism.[1–3] Many microorganisms overcome the threat of F^- toxicity by exporting the anion below inhibitory levels via Fluc type F^- channels.[4,5] Flucs are small, dual-topology electrodiffusive membrane channels with unprecedented selectivity for F^- over Cl^-.[4] Crystal structures of two bacterial Fluc homologues in complex with engineered protein chaperones show homodimeric channels with each subunit oriented antiparallel to its mate and two chaperones bound, one on each end of the channel.[6] These chaperones, termed monobodies,[7] are β-sandwich fold proteins with a type III human fibronectin scaffold and surface loops, much like antibody complementarity-determining regions, which are varied through highly diverse *in vitro* combinatorial libraries, and selected for nanomolar-affinity binding to Fluc.[8] The monobody selection procedure, which diversifies ~20 residues in certain loop and sheet regions, renders Fluc monobodies highly enriched with Tyr and less so with Ser, Phe, and Trp.[8,9]

In addition to serving as crystallization chaperones, mono-bodies also block Fluc-mediated F^- current[4] by occluding the wide vestibules that connect the F^- selective pores to bulk solution. The blocking effect is readily observed by recording single Fluc channels with a monobody present on one side of the membrane, where monobody binding events appear as long-lived nonconducting intervals in the channel record.[8] The diversified paratope, a largely unstructured loop extending deeply into the aqueous vestibule, provides most of the monobody−channel interface.[10]

While the monobody blocking behavior has provided valuable information about Fluc channel mechanisms,[10] it has offered little insight into the intimate interactions at the monobody−channel interface or the energetic contributions of individual residues to the affinity of the complex. Accordingly, this study seeks to understand the molecular and

energetic underpinnings of binding of a monobody to Fluc channels by comparing equilibrium affinities of two monobodies, S9 and S12, selected for “Ec2”, an *Escherichia coli* Fluc homologue (UniProt entry P37002).[4] We also attempt to improve monobody affinity through structure-guided mutagenesis. To do this, structures of Ec2 in complex with monobody S9 or S12 were determined to identify candidate residues for mutagenesis at the monobody—Fluc interface.[8] Then, both S9 and S12 were extensively mutated along the FG loop, and the affinities of each mutant for detergent-solubilized Ec2 were determined using a fluorescence anisotropy (FA) assay. Overall, we found in both monobodies analogous functional paratopes that map well to the structural interface and determined that Tyr residues in each monobody contribute to binding affinity but often withstand substitution by other aromatics without a large disruption of affinity.

MATERIALS AND METHODS

Biochemicals.

All reagents were purchased from Sigma-Aldrich or Fischer Scientific at the highest quality available. 1-Palmitoyl-2-oleoyl-sn-glycero-3-phosphoethanolamine (POPE), 1-palmitoyl-2-oleoyl-*sn*-glycero-3-phospho(1′-*rac*-glycerol) (POPG), and *E. coli* polar lipids (EPL) were purchased from Avanti Polar Lipids. EDANS C2 maleimide was purchased from Molecular Probes, and *n*-decyl maltoside (DM) was purchased from Anatrace.

Expression and Purification of Ec2.

The *E. coli*-optimized Fluc-Ec2 gene with a C-terminal His_6 tag, a short linker, and a functionally nonperturbing R25K mutation, which we here term “wild type” (WT) Ec2, was cloned into a pET-21c(+) vector (Invitrogen) and expressed in *E. coli* BL21-DE3 cells in 1 L terrific broth cultures supplemented with 50 μg/mL ampicillin as previously described.[4] Cells were induced at an A_{600} of 0.8−1 and after being harvested 1 h later were stored overnight at 4 °C. Cell pellets were resuspended in 100 mM NaCl, 50 mM tris(hydroxymethyl)aminomethane hydrochloride (Tris-HCl) (pH 7.5), 1 mM phenylmethanesulfonyl fluoride (PMSF), and 1 μg/mL leupeptin and sonicated for 3 min. The sonicant, extracted at room temperature for 2 h with 3% DM, was clarified by centrifugation at 12000 rpm for 45 min and loaded onto a pre-equilibrated Co-affinity column (Clontech). Ec2 was eluted in 400 mM imidazole, 100 mM NaCl, 20 mM Tris-HCl (pH 7.5), and 5 mM DM. Final purification by size exclusion chromatography on a Superdex S-200 column was completed in 100 mM NaCl, 10 mM NaF, 25 mM [4-(2-hydroxyethyl)-1-piperazineethanesulfonic acid]-NaOH (HEPES-NaOH) (pH 7.0), and 5 mM DM unless otherwise noted.

Expression, Purification, and Fluorophore Conjugation of Monobodies.

The monobody S9 and S12 WT genes with N-terminal His_6 tags and short linkers were cloned into a pET-21a(+) vector and expressed in *E. coli* BL21-(DE3) cells induced with 200 μM isopropyl β-D-1-thiogalactopyranoside (IPTG) in 1 L of terrific broth medium supplemented with 50 μg/mL kanamycin as previously described.[8,11] Point mutations were made using overlap extension polymerase chain reaction and standard DNA subcloning techniques or with the QuikChange (Agilent) kit and confirmed via gene sequencing

(Genewiz). Monobodies used for fluorescence anisotropy and single-channel blocking experiments carried a nonperturbing A12C mutation for fluorophore conjugation. Monobody cultures were grown at 37 °C while being shaken at 220 rpm to an A_{600} of 0.6–0.8 and induced with 200 μM IPTG for 3 h at 30 °C. Cells were then centrifuged at 4500 rpm, and the pellet was resuspended in 100 mM NaCl and 50 mM Tris-HCl (pH7.5) with 1 μg/mL leupeptin and 1 mM PMSF. Cells were broken via sonication for 3 min. The supernatant was clarified via centrifugation for 45 min at 18000 rpm and loaded in batch mode onto a pre-equilibrated Co-affinity column for 1 h at room temperature (Clontech). A room-temperature on-column 16 h digestion with TEV protease harboring a His_6 tag (0.2 mg/L of culture) removed the monobody His_6 tag and linker. The cleaved monobodies were eluted in 100 mM NaCl and 20 mM Tris-HCl (pH 7.0), labeled with EDANS C2 maleimide, and purified via a Superdex S-75 size exclusion column (GE Healthcare) in 100 mM NaCl, 10 mM NaF, and 25 mM HEPES-NaOH (pH 7) unless otherwise noted.[12] Labeled monobodies were stored at concentrations of 75–200 μM in 10% glycerol at −20 °C.

Crystallography of S9-Ec2 and S12-Ec2.

Monobodies S9 WT and S12 WT used for crystallization were purified as described above, with the final size exclusion step being performed in 100 mM NaCl, 10 mM NaF, and 10 mM HEPESNaOH (pH 7.0). The Ec2 channel was purified in the same buffer with 5 mM DM. Following purification, Ec2 and monobodies were concentrated to 10 mg/mL in a 10 kDa molecular weight cutoff centrifugal concentrator, and monobodies were supplemented with 4 mM DM prior to being mixed with Ec2 at a 1:1.2 Ec2:monobody molar ratio. This mixture (1 μL) was added to 1 μL of the crystallization solution in 24-well sitting-drop plates with a 0.3 mL reservoir volume at 22 °C. S9-Ec2 crystals grew in 2–3 weeks in 100 mM N-(2-acetamido)iminodiacetic acid-NaOH (ADA-NaOH) (pH 6.0), 50 mM $LiNO_3$, and 31% PEG 600. S12-Ec2 crystals grew in 3–4 weeks in 50 mM ADA-NaOH (pH 6.2), 50 mM $LiNO_3$, and 34% PEG 400. Both S9-Ec2 and S12-Ec2 were snap-frozen in liquid nitrogen prior to data collection without further cryoprotection. Data sets were collected at the Advanced Light Source on beamline 8.2.2 or 8.2.1. Images were integrated using Mosflm and scaled with Aimless or the Xia2, XDS, and Aimless pipeline.[13–15] Phases were solved via molecular replacement with PHASER using Protein Data Bank (PDB) entry 5KBN as the search model.[16] Refinement was completed using Refmac; real space refinement was performed in COOT, and geometry was validated with Molprobity.[17–19] For analysis of protein interfaces and the surface area involved in crystal structure contacts, PDBePISA was used.[20]

Fluorescence Anisotropy Assay of Ec2−Monobody Binding.

Monobodies used for Ec2 binding experiments were conjugated at an engineered A12C position with EDANS C2 maleimide as previously described.[12] A fixed concentration of fluorophore-labeled monobody (100 nM) in 100 mM NaCl, 10 mM NaF, 25 mM HEPES-NaOH (pH 7), and 5 mM DM was mixed with Ec2 at varying concentrations and incubated at room temperature for 30 min. Fluorescence anisotropy was determined in triplicate at 21–22 °C on a Horriba Fluoromax spectrofluorimeter. Results were fit to single-site binding isotherms with total Ec2 as the experimental variable.[12]

$$A([\mathrm{Ec2}]) = A_o + \frac{A_f - A_o}{2}\left(1 + \frac{[\mathrm{Ec2}]}{[\mathrm{Mb}]} + \frac{K_d}{[\mathrm{Mb}]}\right) \times \left[1 - \sqrt{1 - \frac{4\frac{[\mathrm{Ec2}]}{[\mathrm{Mb}]}}{\left(1 + \frac{[\mathrm{Ec2}]}{[\mathrm{Mb}]} + \frac{K_d}{[\mathrm{Mb}]}\right)^2}}\right] \quad (1)$$

where A_0 and A_f are the initial and final fluorescence anisotropy, respectively, [Mb] is the fixed monobody concentration, and K_d is the dissociation constant. Dissociation constants of mono-body mutants were compared by

$$\Delta\Delta G^\circ = RT \ln \frac{K_{dMut}}{K_{dWT}} \quad (2)$$

Single-Channel Recordings of S9 and S12 Block.

Ec2 for single-channel recordings in planar phospholipid bilayers was prepared via *E. coli* expression and reconstitution into *E. coli* polar lipid (EPL) liposomes or with an *in vitro* synthesis and DMPC nanodisc (ND) reconstitution system. For liposome reconstitution, EPL (dried under N_2 from chloroform stocks) was suspended at a concentration of 10 mg/mL in 100 mM NaCl, 20 mM Tris-HCl (pH 7.0), and 30 mM 3-[(3-cholamidopropyl)dimethylammonio]-2-hydroxy-1-propanesulfonate (CHAPS) and bath sonicated to clarity. Ec2 protein(0.05 μg/mg EPL) was added, and the mixture was extensively dialyzed for 48 h against 100 mM NaCl and 20 mM Tris-HCl (pH 7.0). Liposomes stored in aliquots at −80 °C were frozen and thawed three times prior to use in single-channel recordings.

In vitro synthesis and nanodisc (ND) reconstitution was performed with the Membrane Max HN Protein Expression Kit (Invitrogen) using the Ec2 gene with a stop codon upstream of the His_6 tag and linker in pET-21a(+).[4] Ec2 was expressed in the presence of His_6-tagged NDs and DMPC lipids provided with the kit. The Ec2−ND complexes were purified directly from the *in vitro* synthesis reaction via a HisPur Ni-NTA spin column (Thermo Scientific). The volume was brought to 400 μL with 10 mM imidiazole, 300 mM KCl, and 20 mM NaH_2PO_4-KOH (pH 7.4) and the mixture loaded onto the HisPur column. After incubation at room temperature, the column was washed three times with 400 μL of the solution described above supplemented with 10 mM imidiazole and eluted in 250 mM imidiazole, 300 mM KCl, and 20 mM NaH_2PO_4-KOH (pH 7.4). The purified Ec2−ND complexes were stored at 4 °C until they were used.

For single-channel recording, Ec2 proteoliposomes were thawed, mixed in a 1:1 ratio with 2 M KCl, frozen and thawed, and briefly sonicated immediately before being used. Alternatively, Ec2—ND complexes were diluted 10^5-fold with 1 M KCl. Single Ec2 channels were recorded by adding 0.5 μL of the liposomes or diluted NDs directly to the

planar bilayer.[8] For all monobody blocking experiments, as soon as a Fluc channel appeared, 200–500 nM monobody was stirred into the *cis* chamber to produce single-sided blocking events. Recordings were acquired at a holding voltage of −200 mV with symmetric solutions consisting of 300 mM NaF, 10 mM 3-(N-morpholino)propanesulfonic acid (MOPS)-NaOH (pH 7.0), and 50 μg/mL bovine serum albumin. Electrical ground was defined as the *trans* side of the bilayer. Recordings were sampled at 2 kHz and low pass filtered at 1 kHz during acquisition and digitally filtered to 200–500 Hz for analysis.

Single-channel records were analyzed in Clampfit version 9.1 (Molecular Devices) to derive monobody dwell-time kinetics and dissociation constants from single-exponential fits of cumulative distributions containing 22–143 events. Values representing means ± the standard error of the mean (SEM) of three to five separate channels are reported in Table 1.

RESULTS AND DISCUSSION

To investigate the molecular basis of the 20-fold difference in affinity between the S9 and S12 monobodies, we combined structural analysis with equilibrium binding assays and single-channel recordings to assess the functional effects of point mutations in both S9 and S12. In single-channel recordings (Figure 1A), Ec2 channels in the absence of monobodies are open >98% of the time, displaying infrequent, brief closings. Both monobodies block the channel stochastically, characterized by nonconducting intervals separating channel openings.[8,10,12] Analysis of single-channel block by WT S9 and S12 yields dissociation constants of ~200 and ~10 nM, respectively, with affinity differences expressed mainly in dissociation rates.

The low-throughput nature of single-channel recordings motivated us to use a biochemical assay, fluorescence anisotropy, to quantify dissociation constants of S9 and S12 mutants in a detergent solution (Figure 1B). Dissociation constants derived from each technique (Table 1) agree well for both monobodies.

To identify residues at the monobody—Ec2 channel interface, we crystallized S9—Ec2 and S12—Ec2 complexes from detergent micelles and determined the structures of both complexes (Table 2). These differ from previously deposited Ec2 structures in several ways. While the structure of the Ec2—S12 complex employs a novel monobody, the previously determined structure of the WT Ec2—S9 complex (PDB entry 5A43) includes nonperturbing substitutions that enrich the protein with additional SeMet residues for phasing, and other structures of the Ec2−S9 complex carry functional mutations to critical residues in the F^- conduction pathway.[6,21,22] In the structures presented here (Figure 2), the Ec2 homodimer binds two monobodies, each protruding into a vestibule on either end of the channel. All crystal contacts are mediated by mono-bodies, and the channels in the two structures align precisely [root-mean-square deviation (rmsd) of 0.7 Å]. Each S12 monobody donates ~1800 $Å^2$ of surface area to the channel− monobody interface, dominated by the FG loop extending 16 Å into the channel's aqueous vestibule; the S9−Ec2 interface is slightly smaller (~1720 $Å^2$), but the FG loop protrudes 4 Å more deeply into the channel vestibule. Guided by these structures, we introduced substitutions at all positions along the monobody—channel interfaces. Energetic responses to mutations are grouped

(Tables 3 and 4) by the magnitude of the change in binding free energy relative to that of the WT, with “severe” denoting a ΔΔG° greater than the upper limit of the FA assay (3.4 kcal/mol), “moderate” denoting a ΔΔG° of 0.6−3.4 kcal/mol, and “indifferent” denoting a ΔΔG° of <0.6 kcal/mol. Because monobodies were selected from high-diversity libraries, we also wondered whether it would be possible to improve binding by human-directed mutagenesis.

The structure of the S9−Ec2 complex (Figure 3A) reveals a monobody paratope consisting of six residues located within2.5–4.5 Å of the Ec2 channel: T29 on the scaffold and Y78, Y80, D82, L83, and Y84 on the FG loop (Figure 3A–C). The β-methyl group of T29 (Figure 3C) approaches the Ec2 L90 side chain, while its hydroxyl H-bonds with the carbonyl of P31. Despite these structural features, T29 mutations that remove the hydrophobic or polar contacts or both (T29S, -V, or -A) result in only mild weakening of monobody binding [<1 kcal/mol (Table 3)]. The FG loop carries five Tyr residues, three of which contact Ec2. Each of these was conservatively mutated to Phe to assess H-bond contributions and to Gln to offer alternative H-bonding capability. The Y78F (Figure 3C) mutation moderately weakens binding (~1 kcal/mol) even though its closest Ec2 polar contact, E86, is too far away (4.3Å) for robust H-bonding. Y80F and Y84F are indifferent despite their close polar contacts, 2.7 Å from Ec2 T71 and 2.6 Å from Ec2 Q92. Substitution of Trp and Ile to retain or remove aromaticity and volume leads to indifferent and moderate disruptions. In all cases, Gln substitutions of these Tyr residues severely destabilize monobody binding. The only S9 hydrophobic residue at the interface, L83, tucks between Ec2 F55 and T70; substitution with Phe is moderately disruptive, while substitutions with Ile and Tyr are indifferent. The final S9 residue, D82, situates its carboxylate side chain 4.2 Å from the ε-amino group of Ec2 K66, raising the possibility of a salt bridge buried in a low-dielectric environment. To our surprise, neutralizing the carboxylate with a D82N substitution produces no significant change in affinity.

The monobody S12 paratope has seven amino acids at the Ec2 interface located at positions T29 on the scaffold and Y78, S80, W84, Y85, E86, and Y87 on the FG loop (Figure 4A). It contacts Ec2 through L90, as with S9 (Figure 4C), and the T29V and -S substitutions have similarly negligible or moderate effects on monobody binding. The S12 FG loop contains four Tyr residues, three of which contact Ec2. Conservative Phe mutations are moderately disruptive at positions Y78, Y85, and Y87, while the radical substitution Y78S abolishes binding. Substitution of Y78 with Trp and Ile results in indifferent and moderate disruptions, respectively. As with S9, the Y78 terminal OH group is 4.4 Å from Ec2 E86 while the OH groups of Y85 and Y87 are 2.6 Å from the side chain of Q92 and the carbonyl L56, respectively. A radical mutation, S80A, perched 3.4 Å from the carbonyl of Ec2 N27 neuters the H-bond donor but is nevertheless indifferent in its effect on affinity. Binding also responds only moderately to mutations of E86; located on an elongated β-strand in S12, this carboxylate is ~5 Å from K66, its closest contact in Ec2, and may be neutralized (E86Q) or moved away from its partner (E86D) with moderate effects. Position W84 was probed with W84H to conserve aromatic H-bonding character, W84L to test removal of side chain volume, and W84Y for placement of a bulky H-bond donor. Destabilization of the monobody at this site was severe for W84H and W84L and moderate for W84Y. Table 4 reports affinities and free energy perturbations for S12 mutants.

The structures of the S9—Ec2 and S12—Ec2 complexes are, as expected, similar in fold, the only global difference appearing in the orientation of the monobody on the channel, an ~10° counterclockwise rotation of S12 relative to S9 (Figure 5A).

Local changes are found in the FG loop of S9 and S12 where amino acid similarities diverge (Figure 5B,C). The entering FG loop β-strands of both S9 and S12 are identical in structure, while the β-strand of S12, containing residues W84, Y85, E86, and Y87, is extended two residues higher up the Ec2 vestibule than the S9 β-strand. Ec2 contacts closest to the ascending FG loop β-strand of S12 are the only perturbed residues found on the channel, manifesting in an ~4 Å movement of the side chain of Ec2 L52 (Figure 5D). Fluorescence anisotropy binding isotherms for all mutants are depicted in Figure S1.

The results described here provide a molecular and energetic picture of how synthetically derived monobodies associate with Fluc channels. As expected for a minimalist binding protein, the structural paratopes for both monobodies contain residues that upon mutagenesis disrupt the affinity of the complex, speaking strongly to the efficacy of selection for affinity from highly diverse libraries; in light of the superb diversified libraries provided by the Koide group,[11] it is no surprise that our aim to design higher-affinity monobody mutants failed. None of our substitutions improves binding affinity. We note that Tyr appears far more frequently in the FG loops of both S9 (38%) and S12 (28%) from enrichment during selection than in all proteins, in protein interfaces, or indeed in the monobodies' nondiversified sequences (~5%);[23] however, two Tyr residues in S9 accept Phe and Trp without a large disruption of affinity, suggesting that these side chains contribute space complementarity and weak dispersion forces to the interface. In contrast, the Tyr residues in S12 participate in stronger H-bonding interactions, which could readily account for the 20-fold difference in affinity between monobodies S9 and S12. Without high-resolution structures of the mutants here, it would be idle to speculate about the detailed reasons for the energetic consequences of the mutations; indeed, even with a panoply of mutant structures, such reasons might still be obscure, as in a recent analysis of ion-permeation determinants in this same channel,[22] where the mechanistic crystallographer's dictum "Angstroms are not kilocalories" announces itself loudly.

Supplementary Material

Refer to Web version on PubMed Central for supplementary material.

ACKNOWLEDGMENTS

The authors are grateful to Luci Kolmakova-Partensky and Tania Shane for their assistance with DNA cloning, and the authors acknowledge Drs. Shohei and Akiko Koide for originally selecting the monobodies used here (details in ref 4). The authors also thank the staff at Advanced Light Source beamlines 8.2.2 and 8.2.1 for their technical expertise and ever-helpful presence during data collection. This research used resources of the Advanced Light Source, a U.S. Department of Energy Office of Science User Facility under Contract DEAC02–05CH11231.

Funding

This study was in part supported by National Institutes of Health Grant RO1-GM10723.

REFERENCES

(1). Ji C, Stockbridge RB, and Miller C (2014) Bacterial fluoride resistance, Fluc channels, and the weak acid accumulation effect. J. Gen. Physiol 144, 257–261. [PubMed: 25156118]

(2). Marquis RE, Clock SA, and Mota-Meira M (2003) Fluoride and organic weak acids as modulators of microbial physiology. FEMS Microbiol Rev. 26, 493–510. [PubMed: 12586392]

(3). Samygina VR, Moiseev VM, Rodina EV, Vorobyeva NN, Popov AN, Kurilova SA, Nazarova TI, Avaeva SM, and Bartunik HD (2007) Reversible inhibition of Escherichia coli inorganic pyrophosphatase by fluoride: trapped catalytic intermediates in cryo-crystallographic studies. J. Mol. Biol 366, 1305–1317. [PubMed: 17196979]

(4). Stockbridge RB, Robertson JL, Kolmakova-Partensky L, and Miller C (2013) A family of fluoride-specific ion channels with dual-topology architecture. eLife 2, e01084 DOI: 10.7554/eLife.01084. [PubMed: 23991286]

(5). Baker JL, Sudarsan N, Weinberg Z, Roth A, Stockbridge RB, and Breaker RR (2012) Widespread genetic switches and toxicity resistance proteins for fluoride. Science 335, 233–235. [PubMed: 22194412]

(6). Stockbridge RB, Kolmakova-Partensky L, Shane T, Koide A, Koide S, Miller C, and Newstead S (2015) Crystal structures of a double-barrelled fluoride ion channel. Nature 525, 548–551. [PubMed: 26344196]

(7). Koide S, Koide A, and Lipovsek D (2012) 6 Target-Binding Proteins Based on the 10th Human Fibronectin Type III Domain (10Fn3). Methods Enzymol. 503, 135. [PubMed: 22230568]

(8). Stockbridge RB, Koide A, Miller C, and Koide S (2014) Proof of dual-topology architecture of Fluc F— channels with monobody blockers. Nat. Commun 5, 5120. [PubMed: 25290819]

(9). Koide A, Gilbreth RN, Esaki K, Tereshko V, and Koide S (2007) High-affinity single-domain binding proteins with a binary-code interface. Proc. Natl. Acad. Sci. U. S. A 104, 6632–6637. [PubMed: 17420456]

(10). Turman DL, and Stockbridge RB (2017) Mechanism of single- and double-sided inhibition of dual topology fluoride channels by synthetic monobodies. J. Gen. Physiol 149, 511–522. [PubMed: 28258203]

(11). Koide A, Wojcik J, Gilbreth RN, Hoey RJ, and Koide S (2012) Teaching an old scaffold new tricks: monobodies constructed using alternative surfaces of the FN3 scaffold. J. Mol. Biol 415, 393–405. [PubMed: 22198408]

(12). Turman DL, Nathanson JT, Stockbridge RB, Street TO, and Miller C (2015) Two-sided block of a dual-topology F-channel. Proc. Natl. Acad. Sci. U. S. A 112, 5697–5701. [PubMed: 25902543]

(13). Battye TGG, Kontogiannis L, Johnson O, Powell HR, and Leslie AG (2011) iMOSFLM: a new graphical interface for diffraction-image processing with MOSFLM. Acta Crystallogr., Sect. D: Biol. Crystallogr 67, 271–281. [PubMed: 21460445]

(14). Winter G, Lobley CM, and Prince SM (2013) Decision making in xia2. Acta Crystallogr., Sect. D: Biol. Crystallogr 69, 1260–1273. [PubMed: 23793152]

(15). Kabsch W (2010) XDS. Acta Crystallogr., Sect. D: Biol. Crystallogr 66, 125–132. [PubMed: 20124692]

(16). McCoy AJ, Grosse-Kunstleve RW, Adams PD, Winn MD, Storoni LC, and Read RJ (2007) Phaser crystallographic software. J. Appl. Crystallogr 40, 658–674. [PubMed: 19461840]

(17). Winn MD, Murshudov GN, and Papiz MZ (2003) Macromolecular TLS refinement in REFMAC at moderate resolutions. Methods Enzymol. 374, 300–321. [PubMed: 14696379]

(18). Emsley P, Lohkamp B, Scott WG, and Cowtan K (2010) Features and development of Coot. Acta Crystallogr., Sect. D: Biol. Crystallogr 66, 486–501. [PubMed: 20383002]

(19). Chen VB, Arendall WB, Headd JJ, Keedy DA, Immormino RM, Kapral GJ, Murray LW, Richardson JS, and Richardson DC (2010) MolProbity: all-atom structure validation for macromolecular crystallography. Acta Crystallogr., Sect. D: Biol. Crystallogr 66, 12–21. [PubMed: 20057044]

(20). Krissinel E, and Henrick K (2007) Inference of macro-molecular assemblies from crystalline state. J. Mol. Biol 372, 774–797. [PubMed: 17681537]

(21). Last NB, Kolmakova-Partensky L, Shane T, and Miller C (2016) Mechanistic signs of double-barreled structure in a fluoride ion channel. eLife 5, e18767 DOI: 10.7554/eLife.18767. [PubMed: 27449280]

(22). Last NB, Sun S, Pham MC, and Miller C (2017) Molecular determinants of permeation in a fluoride-specific ion channel. eLife 6, e31259 DOI: 10.7554/eLife.31259. [PubMed: 28952925]

(23). Yan C, Wu F, Jernigan RL, Dobbs D, and Honavar V (2008) Characterization of Protein−Protein Interfaces. Protein J. 27, 59–70. [PubMed: 17851740]

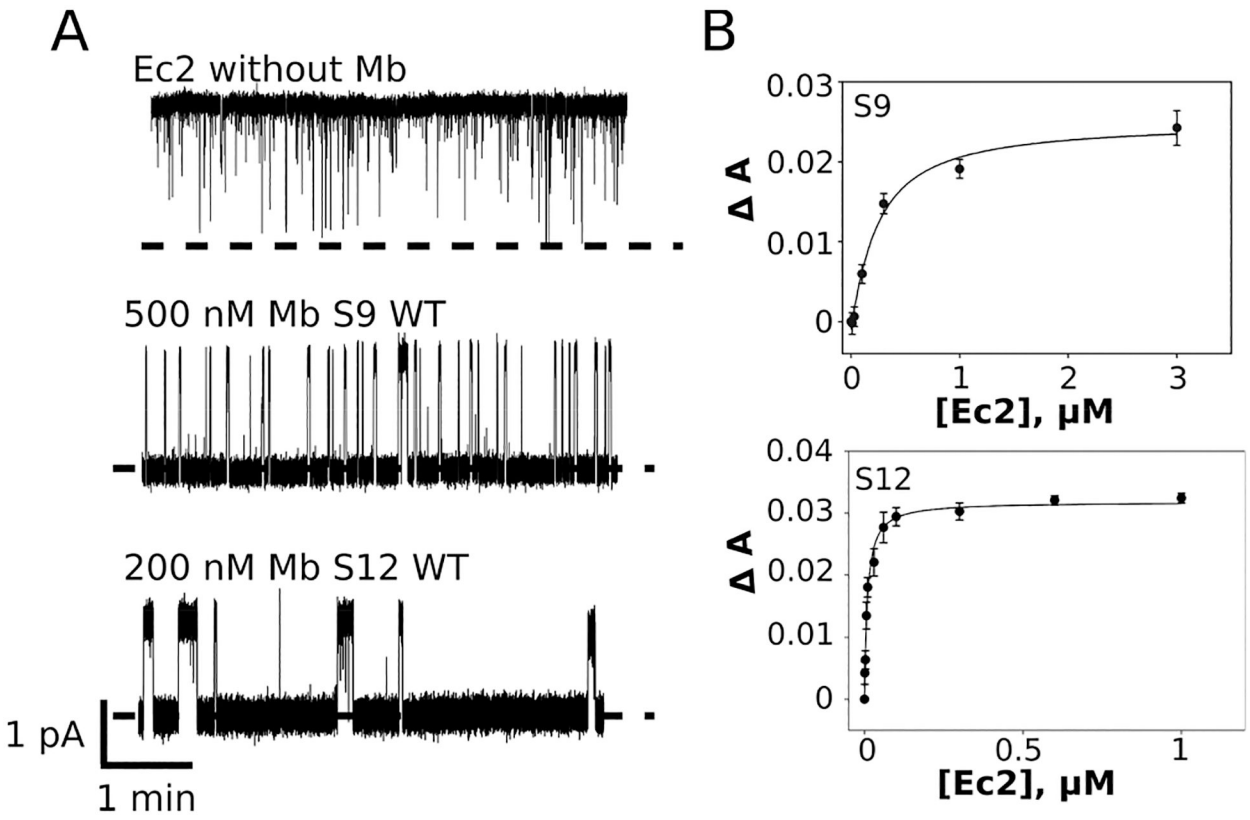

Figure 1.

Binding of monobody blockers to a Fluc F^- channel. (A) Single Ec2 channels in the absence or presence of monobodies S9 and S12 as indicated. Channel openings are upward, and the dashed line denotes the nonconducting level. S9 dwell-time kinetics and affinities are reported in Table 1. (B) FA binding isotherms for S9 and S12 as indicated by the change in anisotropy (ΔA) as Fluc is added. Points and error bars represent means ± SEM ($N = 3$) with the solid curve fit from eq 1. Affinities are reported in Tables 3 and 4.

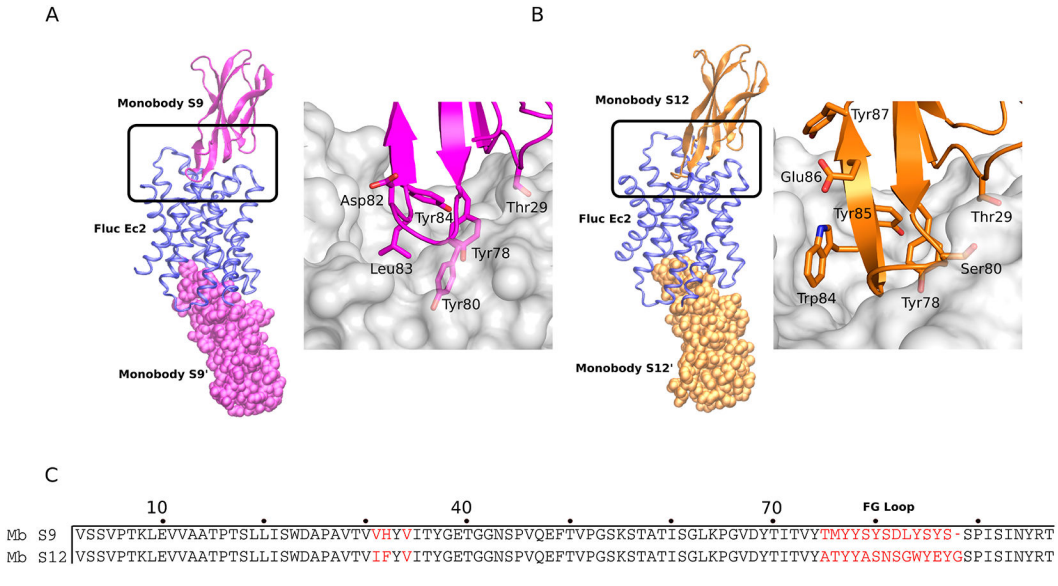

Figure 2.

S9—Ec2 and S12—Ec2 crystal structures. (A and B) Structures of S9—Ec2 (PDB entry 6BX4) and S12—Ec2 (PDB entry 6BX5) complexes, respectively, including monobodies (S9 in magenta and S12 in orange) bound to both ends of the Ec2 channel (blue). Single paratopes are shown in side panels with Ec2 channels depicted as molecular surfaces. (C) Sequence alignment of S9 and S12 with residues varied during selection colored red. Data collection and refinement statistics are reported in Table 2.

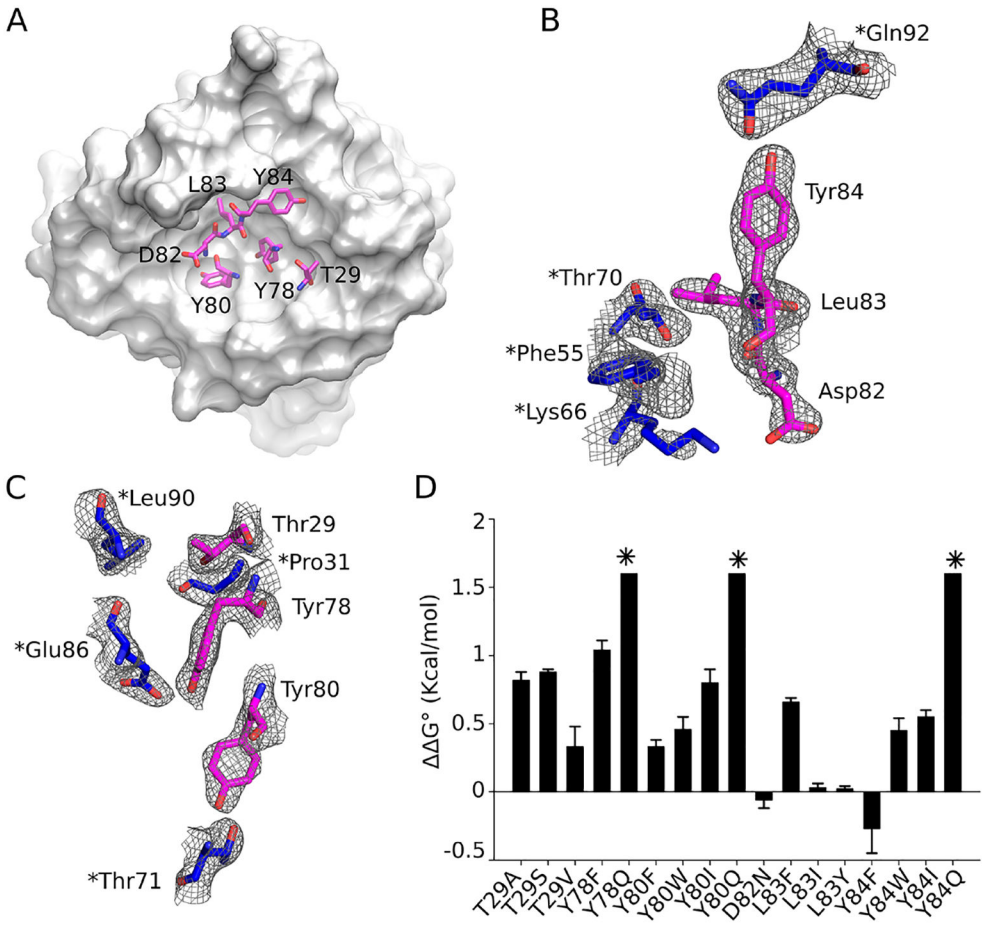

Figure 3.

S9—Ec2 paratope and affinities. (A) S9—Ec2 paratope with interfacial S9 residues on a solvent accessible surface of Ec2. (B and C) Detailed depiction of S9 (magenta) and Ec2 (blue) residues with $2F_o - F_c$ density contoured at 2σ and Ec2 residues labeled with an asterisk. (D) FA-derived ΔΔG° values for S9 mutations with an asterisk indicating the upper assay limit. FA curves depicted in Figure S1.

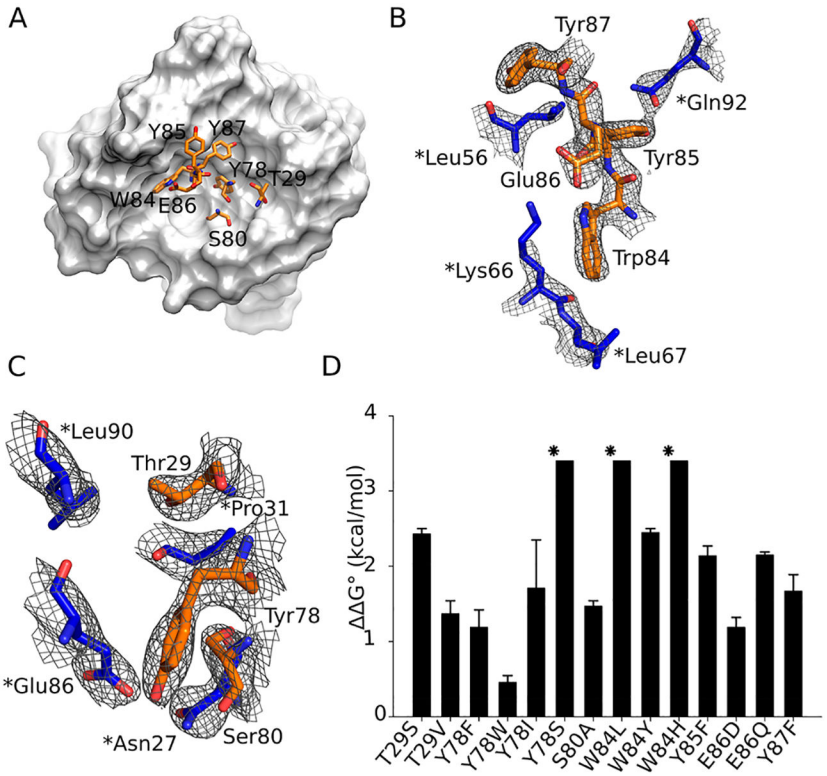

Figure 4.

S12—Ec2 polar contacts and mutagenesis. (A) S12—Ec2 paratope with interfacial S12 residues on a solvent accessible surface of Ec2. (B and C) Detailed depiction of S12 (orange) and Ec2 (blue) residues with $2F_o - F_c$ density contoured at 2σ and asterisks denoting Ec2 residues. (D) FA-derived ΔΔG° values for S12 mutations with asterisks indicating the upper limit of the assay. FA curves depicted in Figure S1.

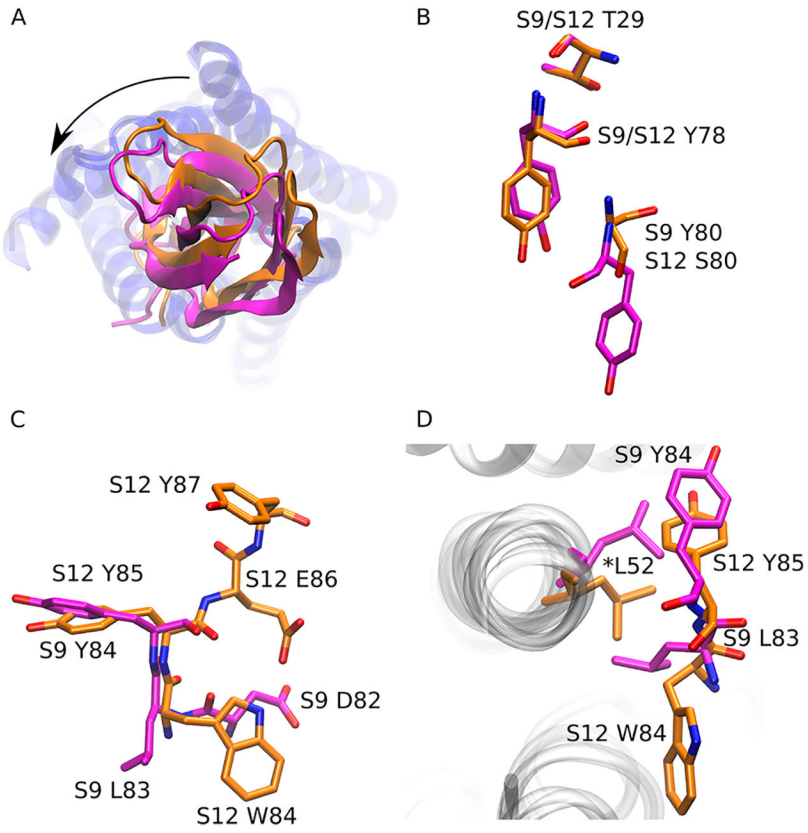

Figure 5.

Structural comparison of S9—Ec2 and S12—Ec2 complexes.(A) Top-down view of aligned structures of S9− and S12−Ec2 complexes showing an ~10° rotation of monobodies. Ec2 channels aligned in blue, S9 in magenta, and S12 in orange. (B and C) Detailed alignment of S9 and S12 structural paratopes. (D) Aligned structures of S9— and S12—Ec2 complexes in white showing Ec2 L52 (indicated with an asterisk with corresponding monobody colors) for both channel structures and the S9 and S12 paratopes at this position.

Table 1.

Single-Channel Monobody Block[a]

monobody	τ_{block} (s)	τ_{open} (s)	K_d (nM)
S9	7 ± 2	4 ± 2	210 ± 60
S12	98 ± 22	7 ± 1	14 ± 4

[a]Single-channel dwell-time kinetics and affinities calculated from recordings with 500 nM S9 (34–143 events) and 200 nM S12 (22–53 events). Mean ± SEM reported for three or four independent single channels.

Table 2.

Data Collection and Refinement Statistics

	S9-Ec2 (6BX4)	S12-Ec2 (6BX5)
	Data Collection	
space group	$P4_1$	$P4_12_12$
cell dimensions		
a, *b*, *c* (Å)	87.41, 87.41, 144.33	105.74, 105.74, 183.69
α, *β*, *γ* (deg)	90, 90, 90	90, 90, 90
resolution (Å)	87.41 (2.55)	74.77 (3.00)
R_{merge}	0.096 (1.453)	0.031 (2.008)
R_{meas} [a]	0.103 (1.558)	0.033 (2.083)
$CC_{1/2}$	0.999 (0.956)	0.999 (0.748)
$I/\sigma(I)$	55.4 (2.1)	77.6 (2.1)
completeness (%)	0.999 (1)	0.995 (1)
multiplicity	15.0 (15.2)	24.9 (26.1)
	Refinement	
resolution (Å)	84.34 (2.55)	74.01 (3.00)
no. of reflections	35210	21577
R_{work}/R_{free}	0.223/0.249	0.226/0.253
Ramachandran plot, favored (%)	96.1	96.1
Ramachandran plot, outliers (%)	0.00	0.00
rmsd		
bond lengths (Å)	0.0149	0.0112
bond angles (deg)	1.582	1.734

[a] Multiplicity-independent: $R_{meas} = \sum\left[\sqrt{(N/N-1)}\left(\left|I_{hl} - \langle I_h \rangle\right|\right)/\sum\langle I_h \rangle\right]$.

Table 3.

S9 Monobodies and Mutant Affinities[a]

monobody	K_d (nM)	$\Delta\Delta G°$ (kcal/mol)
WT	210 ± 70	–
T29A	850 ± 100	0.82 ± 0.06
T29S	930 ± 40	0.88 ± 0.02
T29V	370 ± 100	0.3 ± 0.2
Y78F	1230 ± 150	1.04 ± 0.07
Y78Q	>3000	>1.6
Y80F	370 ± 30	0.33 ± 0.05
Y80W	460 ± 70	0.46 ± 0.09
Y80I	800 ± 130	0.8 ± 0.1
Y80Q	>3000	>1.6
D82N	190 ± 40	−0.06 ± 0.06
L83F	640 ± 30	0.66 ± 0.03
L83I	220 ± 10	0.03 ± 0.03
L83Y	220 ± 35	0.02 ± 0.02
Y84F	130 ± 20	−0.3 ± 0.2
Y84W	460 ± 80	0.45 ± 0.09
Y84I	540 ± 40	0.55 ± 0.05
Y84Q	>3000	>1.6

[a]Equilibrium dissociation constants (mean ± SEM) from three independent FA experiments. Positive ΔΔG° values indicate weakening of affinity.

Table 4.

S12 Monobodies and Mutant Affinities[a]

monobody	K_d (nM)	ΔΔG° (kcal/mol)
WT	10 ± 6	–
T29S	620 ± 80	2.43 ± 0.07
T29V	112 ± 34	1.4 ± 0.2
Y78F	88 ± 37	1.2 ± 0.2
Y78W	22 ± 5	0.46 ± 0.09
Y78I	180 ± 80	1.7 ± 0.6
Y78S	>3000	>3.4
S80A	122 ± 15	1.47 ± 0.07
W84L	>3000	>3.4
W84Y	628 ± 50	2.45 ± 0.05
W84H	>3000	>3.4
Y85F	386 ± 89	2.1 ± 0.1
E86D	265 ± 49	1.2 ± 0.1
E86Q.	378 ± 78	2.15 ± 0.04
Y87F	196 ± 73	1.8 + 0.2

[a]Equilibrium dissociation constants (mean ± SEM) from three independent FA experiments. Positive ΔΔG° values indicate weakening of affinity.